PRAMANA — journal of physics



Vol. 84, No. 4
April 2015
pp. 621–635

# Influence of Cu doping on the structural, electrical and optical properties of ZnO

ARINDAM GHOSH[1,2], NAVNITA KUMARI[1] and AYON BHATTACHARJEE[1,3,*]

[1]Department of Physics, National Institute of Technology, Silchar 788 010, India
[2]Department of Physics, Don Bosco College, Tura 794 002, India
[3]Department of Physics, National Institute of Technology Meghalaya, Shillong 793 003, India
*Corresponding author. E-mail: ayonbh@gmail.com

MS received 20 December 2013; revised 29 April 2014; accepted 13 May 2014
**DOI:** 10.1007/s12043-014-0851-1; ***e*Publication:** 30 November 2014

**Abstract.** Pure and Cu-doped zinc oxide (ZnO) nanoparticles were prepared using a chemical method. The dopant concentration (Cu/Zn in atomic percentage (wt%)) is varied from 0 to 3 wt%. Structural characterization of the samples performed using X-ray diffraction (XRD) confirmed that all the nanoparticles of zinc oxide are having polycrystalline nature. Morphological studies were conducted using field emission scanning electron microscopy (FESEM) to confirm the grain size and texture. Electrical measurements showed that the AC conductivity initially decreases and then rises with increasing Cu concentration. The UV–Vis studies showed absorbance peaks in the 200–800 nm region. It is found that the absorbance does not significantly change with doping. This fact is further confirmed from the band-gap calculations using the reflectance graphs. When analysed in terms of Burstein–Moss shift, an increase of band gap from 3.42 to 3.54 eV with increasing Cu concentration is observed. In the photoluminescence (PL) studies a red-shift is observed with increasing dopant concentration.

**Keywords.** Zinc oxide; Cu doping; structural; electrical; optical properties.

**PACS Nos 78.55.Et; 78.40.−q; 81.40.Rs; 81.40.Tv**

## 1. Introduction

Metal oxides like zinc oxide (ZnO), tin oxide ($SnO_2$) and indium oxide ($In_2O_3$) in their pure form and also in doped forms have been extensively investigated in recent years [1–8]. Among these, ZnO has gained prominence because of its abundance and non-toxicity and also because it is inexpensive compared to others. Zinc oxide (ZnO) is a II–VI semiconductor with a wide band gap of 3.37 eV and a large exciton binding energy of 60 meV at room temperature [9]. Nanoparticles of ZnO are used in a variety of applications: They can be used as UV absorbent, antibacterial treatment material [10], catalytic agent [11,12] and as an additive material in several industrial products. It is currently

being used in the fabrication of solar cells [13], gas sensors [14,15], luminescent materials [16], transparent conductors [17], heat mirrors and coatings [18]. Methods such as pulsed laser deposition [19,20], vapour phase transport [21] and chemical vapour deposition [22] have been developed for the preparation of nanostructures of ZnO. Sol–gel method is one of the most important wet chemical methods used for the preparation of metal oxide nanoparticles [23].

Many physical properties of ZnO, such as piezoelectricity, electrical conductivity and defect structures, are greatly influenced by the presence of impurity [24]. Several dopants (Fe, Cr, Al, Cu, Co, Mn, Mg, S, P, etc.) can lead to an increase in the surface area of the ZnO-based powders. The dopants stabilize the ZnO surface, and they also promote changes in the grain size. It was reported that $Fe^{3+}$-doped ZnO nanoparticles with lower crystallinity and high surface area have higher catalytic activity and sensitivity than that of either the pure ZnO or $Fe_2O_3$ [25]. The dielectric properties of pure ZnO are dependent on the presence of interstitial zinc atoms and lack of oxygen at O sites. As pure ZnO is sensitive to oxidation, absorption of $O_2$ results in a decrease of its dielectric properties. Therefore, different dopants have been introduced into ZnO to modify its dielectric and other properties depending on the desired applications. In many cases, when ZnO has been doped, the dielectric properties were reported to be changed because of the extrinsic defects [26].

This study is aimed at the characterization of pure and Cu-doped ZnO nanoparticles synthesized by the chemical method. The dopant concentration of Cu was varied over the range 0–3 wt%. Structural and morphological characterizations of the samples were performed using powder X-ray diffraction (XRD) and field emission scanning electron microscopy (FESEM), respectively. Electrical properties were investigated using inductance capacitance resistance (LCR) measurements and optical properties by UV–Visible (UV–Vis) and photoluminescence (PL) spectroscopy. The influence of Cu on the structural, electrical and optical properties is discussed in this paper.

## 2. Experimental

Zine oxide (ZnO) powder was prepared by the chemical precipitation method and copper chloride ($CuCl_2{\cdot}H_2O$) was used as the source of the dopant. All the reagents were purchased from Merck India Limited and of AR grade. Zinc acetate $Zn(CH_3COO)_2$ was taken as the precursor and ammonium hydroxide ($NH_4OH$) was taken as the precipitating agent. In this reaction, ammonium acetate provides the hydroxyl ions which plays an important role in capping the size of the particles by excluding the agglomeration of the ZnO particles. The pH of the solution was maintained at 8 by adding suitable amounts of ammonium hydroxide. The following chemical reactions take place:

$$Zn(CH_3COO)_2 + NH_4OH \rightarrow Zn^{2+} + 2(CH_3COO)^-,$$

$$CH_3CH_2CH_2{-}NH_2 + H_2O \rightarrow CH_3CH_2CH_2{-}NH^{3+} + OH^-,$$

$$Zn^{2+} + 2OH^- \rightarrow Zn(OH)_2 \rightarrow ZnO + H_2O.$$

The resulting precipitate from the reaction was collected and thoroughly washed several times with distilled water and ethanol to remove traces of chlorides. Chlorides were

formed because $CuCl_2 \cdot H_2O$ was the dopant source and the presence of these chlorides severely impaired the functionality of doped ZnO. The as-prepared sample was then dried in an oven for 4 h. The ZnO powder thus obtained was pelletized at a pressure of ∼13 MPa to form cylindrical pellets. The pellets were annealed at ∼850°C for 12 h in air to improve the crystallinity. Sintered pellets were then polished into discs of 13 mm diameter and 2 mm thickness.

Structural analysis of the pellets was done using PANalyticalX'Pert Pro X-ray Diffractometer with Cu $K_\alpha$ radiation ($\lambda = 0.15418$ nm) as X-ray source at 40 kV and 30 mA at scanning angle ($2\theta$) from 20° to 90°. The samples were also studied using FESEM along with the EDS (ZEISS ULTRA 55) to verify the particle size and composition, respectively. Electrical properties (ac conductivity) were measured using the LCR meter Hi-tester (Model:3522-50 Hioki, Japan) over the frequency range 100 Hz–100 kHz at room temperature with an AC bias of 0.1 mV. For the AC measurements, the flat faces of the pellet were coated with a thin layer of highly conductive silver paste. The pellet was then mounted on a home-made two-probe assembly which was inserted coaxially inside a resistance-heated furnace. UV–Vis studies were performed using CARY 100 Bio UV Visible spectrophotometer (Varian EL 06053308) and PL studies were carried out using Perkin Elmer LS spectrophotometer.

## 3. Results and discussion

### 3.1 *Structural and morphological studies*

The phase purity and structural parameters are obtained from the powder XRD diffraction patterns. The XRD patterns recorded from undoped and doped pellets with different copper concentration are shown in figure 1. Peaks are found to be quite sharp and intense which implies high crystallinity of samples. The XRD pattern of undoped ZnO is found to match with the ICDD reference pattern (01-070-8072) of ZnO. The analysis of diffraction peaks has revealed the presence of ZnO phase for all the compositions. This indicates that the $Cu^{2+}$ ions are substituted with $Zn^{2+}$ ions without any serious effect on the crystalline structure of ZnO. The ionic radius of $Cu^{2+}$ (0.073 nm) is very close to that of $Zn^{2+}$ (0.074 nm), due to which Cu can easily penetrate into ZnO crystal lattice.

The crystallite size $D$ is calculated using the Debye–Scherrer formula

$$D = \frac{0.89\lambda}{\beta \cos\theta}, \tag{1}$$

where $\lambda$ is the X-ray wavelength, $\beta$ is the peak FWHM corrected for instrumental broadening and $\theta$ is the angle at which the peak occurs. For undoped ZnO, $\beta = 0.0787$, $2\theta = 36.3506$; for 1 wt% Cu-doped ZnO, $\beta = 0.096$, $2\theta = 36.2757$ and for 3 wt% Cu-doped ZnO, $\beta = 0.0787$ and $2\theta = 36.1435$, respectively.

The lattice parameters are calculated using Le-Bail and Pawley refinement method. Table 1 shows the unit cell parameters $a$ and $c$ obtained from the XRD data for all the samples. Lattice parameters $a$ and $c$ are found to be slightly greater for Cu-doped samples as compared to those of undoped ZnO. This is due to a slight mismatch in ionic radii between $Zn^{2+}$ and $Cu^{2+}$. The possible error range for each parameter is about ±0.5%. However, there is a systematic variation in lattice parameters with increasing Cu content.

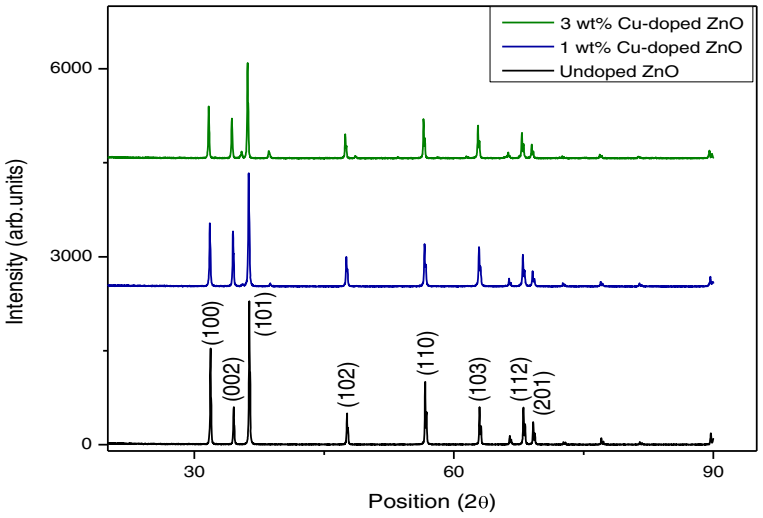


**Figure 1.** XRD patterns recorded from undoped, 1 wt% Cu-doped and 3 wt% Cu-doped ZnO.

The $c/a$ parameter has also been found to show a good match with the value for ideally close packed hexagonal structure (1.6333). The volume of the unit cell for hexagonal system has been calculated using the following equation [27]:

$$V = 0.866a^2c. \tag{2}$$

The bond length $L$ for Zn–O is given by [28]

$$L = \left[\frac{a^3}{3} + \left(\frac{1}{2} - u\right)^2 c^2\right]^{1/2}. \tag{3}$$

The parameter $u$ in the wurtzite structure is given by

$$u = \frac{a^2}{3c^2} + 0.25. \tag{4}$$

The Zn–O bond lengths of undoped and Cu-doped ZnO are given in table 1. It is observed that with the increase in Cu content, bond length increases which is attributed to the segregation of Cu [29,30]. This is visible as some low-intensity peaks in XRD as the dopant

**Table 1.** Bond lengths of undoped, 1 wt% Cu and 3 wt% Cu-doped ZnO.

| Sample | $a$ (Å) | $c$ (Å) | $c/a$ | Volume (Å$^3$) | Zn–O bond length (Å) |
|---|---|---|---|---|---|
| Undoped ZnO | 2.80850 | 5.19494 | 1.849721 | 35.48520 | 1.804848 |
| 1 wt% Cu-doped ZnO | 2.81524 | 5.20470 | 1.848759 | 35.72271 | 1.808766 |
| 3 wt% Cu-doped ZnO | 2.82667 | 5.22554 | 1.848656 | 36.15757 | 1.816065 |

concentration increases. This suggests that the crystalline quality of ZnO is improved by Cu doping.

The samples were also studied using FESEM in order to confirm the particle size. Figures 2a–2c show the FESEM micrographs of undoped ZnO, 1 wt% Cu-doped ZnO and 3 wt% Cu-doped ZnO. The figure clearly shows the formation of ZnO nanoparticles for both undoped and doped samples. From the FESEM images it is also seen that there is a wide variation in the particle size though the textures remain more or less consistent. These images also reveal that the particle size decreases with dopant concentration. A thorough analysis of the images was done using the image processing software, 'ZEN' wherein parameters like average particle size was calculated, which is reported in table 2. It is clearly observed that there is a small deviation in the particle size reported using FESEM data as compared to DS (Debye–Scherrer) or WH (Williamson–Hall) data. However, this is expected as DS calculations do not include changes due to strain whereas WH method is an indirect method where the strain is calculated theoretically. We also observed that similar to DS and WH results, the sizes of the doped ZnO particles obtained by FESEM are smaller than the undoped ZnO particles. The energy dispersive spectroscopy (EDS) results, as shown in figures 2d–2f verify that the samples contain ZnO and Cu only and no other impurities.

A mathematical expression relating the crystallite size and strain-induced broadening was proposed by Williamson and Hall. According to this expression, the peak width as a function of diffraction angle $2\theta$ is considered for analysing X-ray peak broadening [31,32]. The relation is given as

$$\frac{\beta \cos\theta}{\lambda} = \frac{1}{D} + \frac{\varepsilon \sin\theta}{\lambda}, \tag{5}$$

where $\beta$ is the FWHM (rad), $D$ is the crystallite size (nm), $\lambda$ is the X-ray wavelength and $\varepsilon$ is the strain induced on the particles.

Plots shown in figure 3 are drawn with $\sin\theta/\lambda$ along the $x$-axis and $\beta\cos\theta/\lambda$ along the $y$-axis for high intense peak and, thus, the crystallite size and strain of ZnO−Cu can be obtained from the inverse of the intercept at the $y$-axis and slope, respectively. The average crystallite size and strain estimated from the Scherrer relation and WH plot are compared in table 2. The difference in crystallite size estimated from Scherrer relation and that from WH plot calculation is mainly attributed to the inclusion of strain in the as-synthesized sample materials and their estimated strain values are reasonable. The possible error range for crystallite sizes is calculated and they are in the range of $\pm 0.55\%$. Thus, WH plot serves as an additional tool to evaluate and deconvolute crystallite size and strain-induced broadening. The calculated strain is found to be very small in undoped and Cu-doped ZnO samples. This explains why no significant change was observed in XRD pattern. Here, tensile strain is due to an increase in doping concentration and the possible error range estimated is about 0.0050%.

## 4. Electrical studies

AC conductivity is determined using the relation

$$\sigma_{\mathrm{AC}} = C\omega \tan\delta, \tag{6}$$

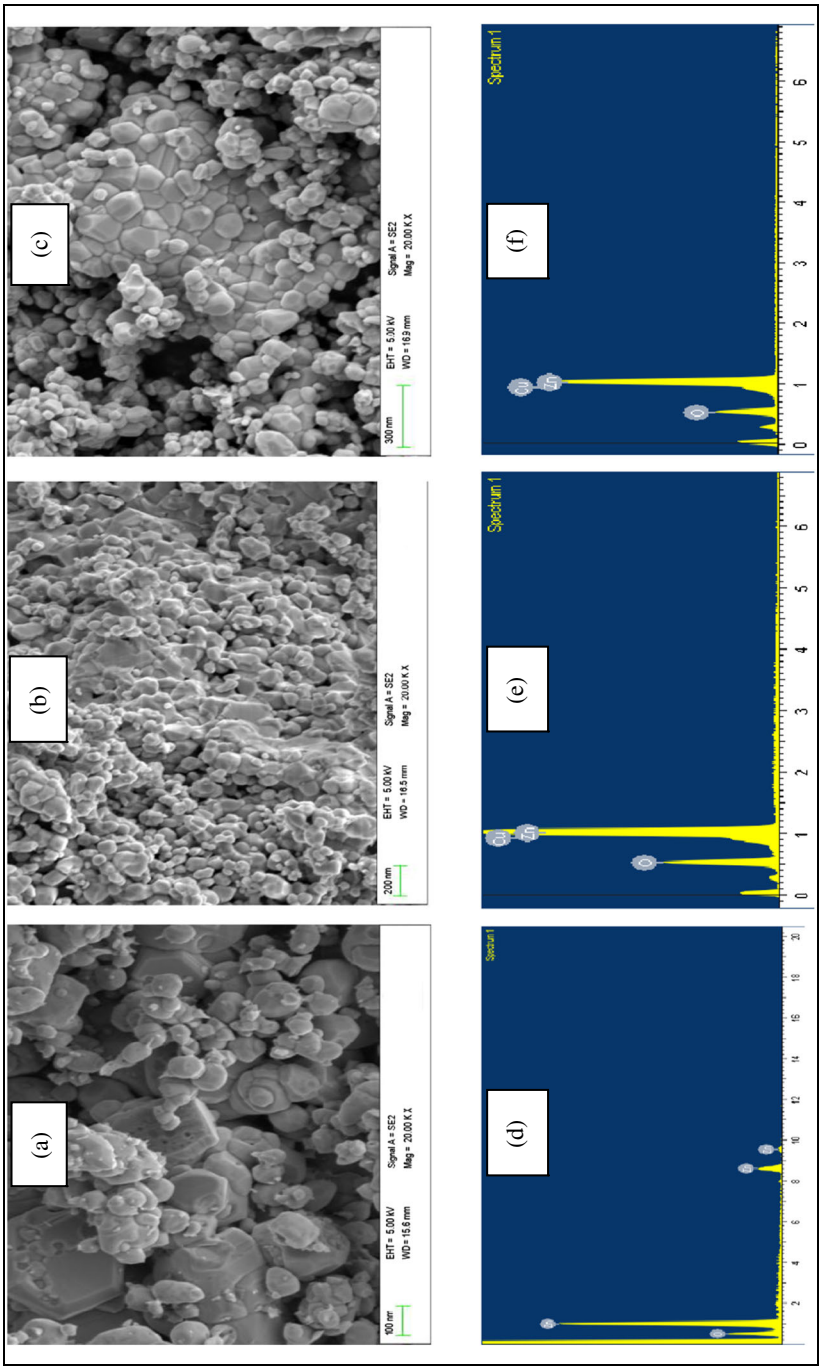


**Figure 2.** FESEM images of (**a**) undoped ZnO, (**b**) 1 wt% Cu-doped ZnO and (**c**) 3 wt% Cu-doped ZnO and EDS of (**d**) undoped ZnO, (**e**) 1 wt% Cu-doped ZnO and (**f**) 3 wt% Cu-doped ZnO.

**Table 2.** Strain calculations of undoped, 1 wt% Cu and 3 wt% Cu-doped ZnO.

| Sample | Intercept | Slope | Average particle size (from FESEM) (nm) | Crystallite size (by Debye–Scherrer) (nm) | Crystallite size (by W–H plot) (nm) | Strain |
|---|---|---|---|---|---|---|
| Undoped ZnO | 0.00634 | 0.000928 | 96.08 | 86.09 | 157.73 | 0.000232 |
| 1 wt% Cu-doped ZnO | 0.00637 | 0.00106 | 95.58 | 82.19 | 156.99 | 0.000265 |
| 3 wt% Cu-doped ZnO | 0.00674 | 0.00111 | 91.79 | 74.14 | 148.37 | 0.000278 |

where $C$ is the capacitance, $\omega$ is the angular frequency and tan $\delta$ is the loss factor.

The dependence of $\sigma_{AC}$ on temperature is given by the relation

$$\sigma_{AC} = \sigma_0 e^{-E_{AC}/kT}, \tag{7}$$

where $\sigma_0$ is the pre-exponential factor, $k$ is the Boltzmann's constant and $E_{AC}$ is the thermal activation energy.

AC measurements are important means for studying the dynamic properties (conductance, capacitance and dielectric loss tangent) of the semiconducting and dielectric materials. They provide information about the interior of the materials in the region of relatively low conductivity. This measurement also helps to distinguish between localized and free band conduction. In localized conduction, the AC conductivity increases with frequency, while in the free band conduction, the conductivity decreases with frequency [33–35]. Further, impedance spectroscopy is a well-known and powerful technique for

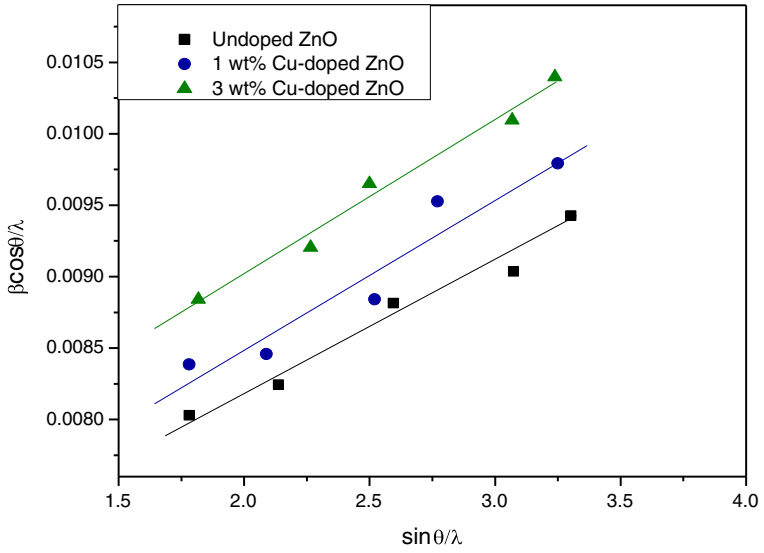


**Figure 3.** Williamson–Hall plots of undoped, 1 wt% Cu-doped and 3 wt% Cu-doped ZnO.

investigating polycrystalline materials where the contribution of various processes such as bulk conduction, grain boundary conduction and transport across electrode–sample interface can be resolved in the frequency domain [36–39].

The frequency dependence of AC conductivity in undoped ZnO and doped ZnO pellets at room temperature is shown in figure 4. It is seen that the AC conductivity increases slightly with frequency. This type of frequency response indicates localized conduction in the ZnO samples, where AC conductivity increases with frequency.

Higher conductivity is found in pure ZnO and the level decreases with the increase in Cu doping. This may be attributed to the fact that the Cu dopant introduces defect ions (such as zinc interstitials and oxygen vacancies) in the ZnO system. These defects tend to segregate at the grain boundaries due to diffusion processes resulting from sintering and cooling. Thus, doping increases the defect concentration and facilitates the formation of grain boundary defect barrier for carriers. This, in turn, decreases the conductivity of the system on doping. However, when the doping level of Cu is high, more Cu ions would get segregated at the grain boundaries. So the density of electrical carriers at the grain boundaries would be high, and the resistance of the grain boundaries would be reduced, thus decreasing the barrier height. In such cases, the doping of Cu has a negative effect on the nonlinear coefficient of the mother sample (ZnO) thereby increasing the conductivity [40,41]. Thus, the AC conductivity is enhanced as the percentage of doping increases from 1 to 3 wt%.

The variations of impedance, tangent loss and capacitance with frequency in pure and Cu-doped ZnO are shown in figure 5. Figure 5a shows that at 1 wt% Cu doping the impedance increases or in other words, the conductivity decreases. However, at higher

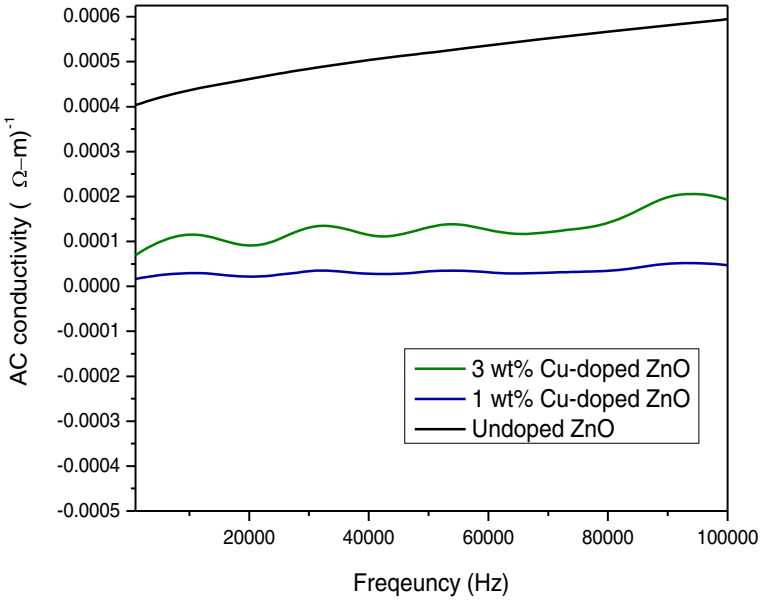


**Figure 4.** Variation of AC conductivity with frequency in undoped, 1 wt% Cu-doped and 3 wt% Cu-doped ZnO.

doping the impedance decreases. This is consistent with the scenario that was observed in case of AC conductivity and which was already explained earlier. Figures 5b and 5c show the variations of tangent loss and capacitance with frequency. From eq. (6), it can be observed that AC conductivity is directly proportional to the tangent loss (tan $\delta$) and also to the capacitance. Consistent with the trend predicted by eq. (6), the variations of the tangent loss and capacitance also show a decrease at 1 wt% Cu doping and then an

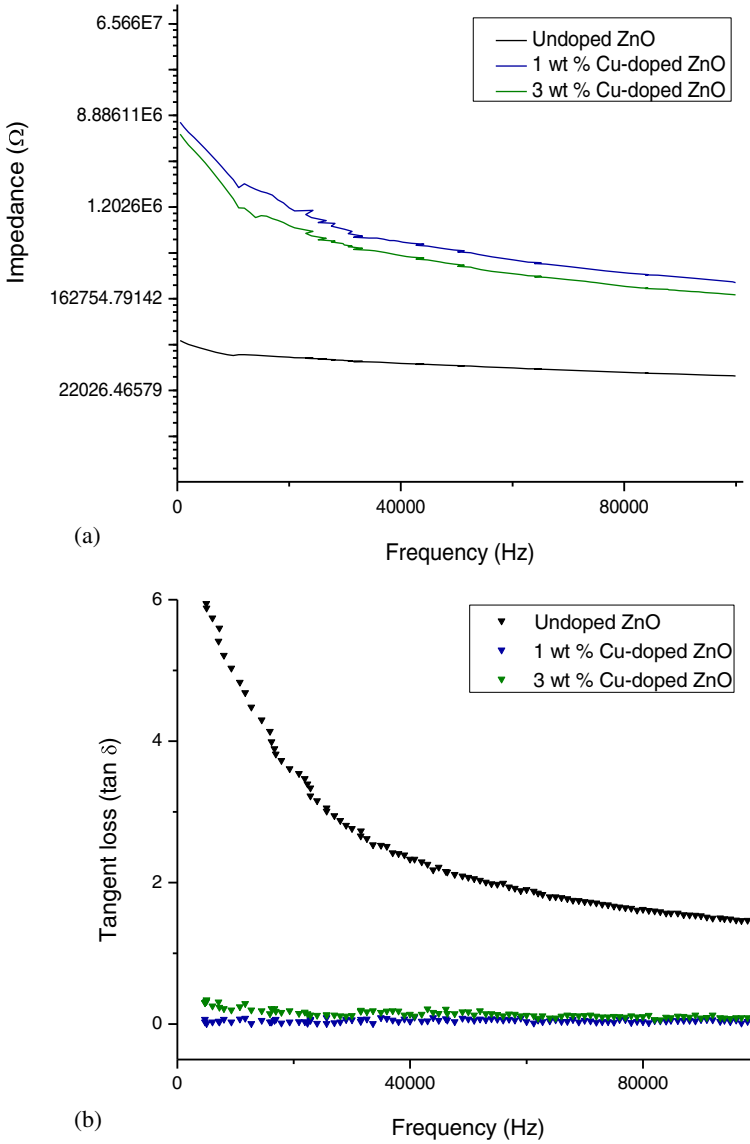


**Figure 5.** Variation of (**a**) impedance, (**b**) tangent loss, (**c**) capacitance with frequency in undoped, 1 wt% Cu-doped and 3 wt% Cu-doped ZnO.

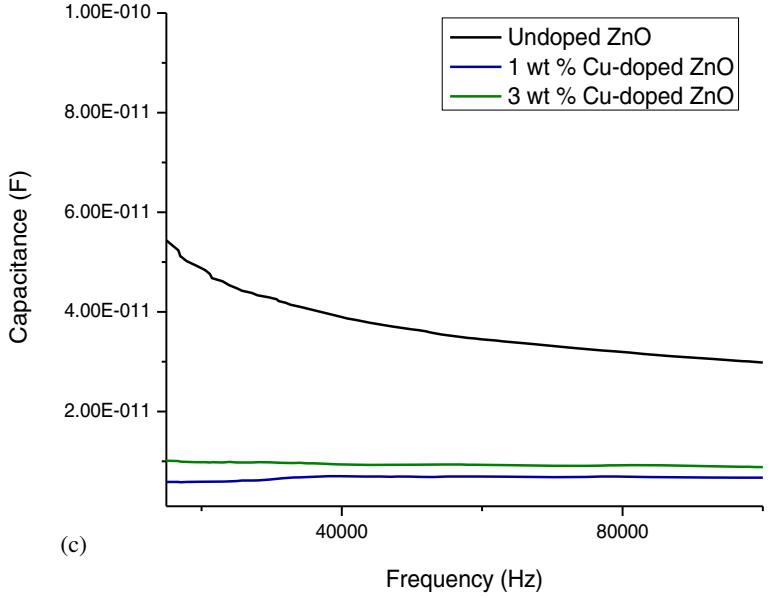


**Figure 5.** *Continued*

increase at 3 wt% Cu doping. These changes in impedance, tangent loss and capacitance provide further evidence to support our explanations provided for the results of AC conductivity.

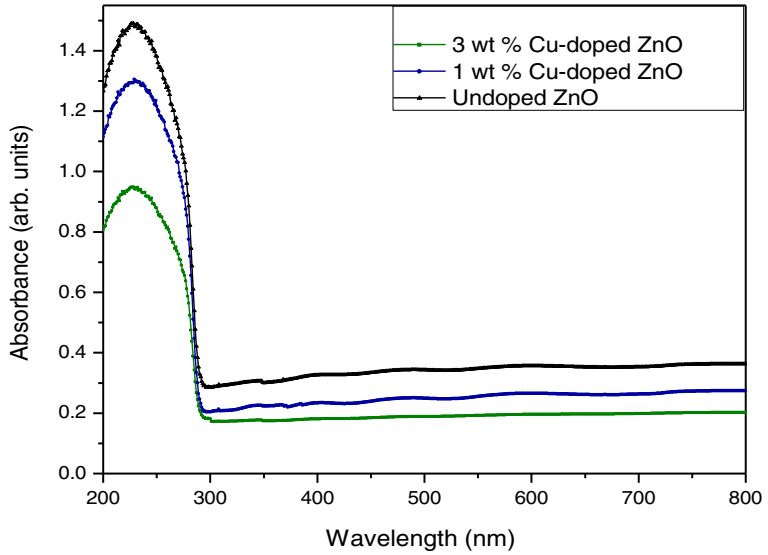


**Figure 6.** Variation of absorbance with wavelength for undoped, 1 wt% Cu-doped and 3 wt% Cu-doped ZnO.

## 5. Optical studies

### 5.1 *UV–Vis studies*

UV–Visible studies are conducted with an intention of measuring the optical band gap of nanocrystals. The transition energy can be easily deduced from the zero crossing of the second derivative of the absorption spectrum. According to the Fermi exclusion principle, for higher photon energies, optical transitions can only occur from the valence band upto the conduction band. The variation of absorbance with wavelength for all the samples is shown in figure 6. It is found that the absorbance initially decreases sharply and then increases slightly. The sharp increase in absorbance at $\lambda < 300$ nm is due to interband transitions at the fundamental edge [42]. Band-gap energy increases with decreasing particle size due to quantum size effects. Substitution of $Zn^{2+}$ by $Cu^{2+}$ results in an increase in oxygen vacancies and electron concentration due to the electronegativity and ionic radius. This increase in carrier density results in the lifting of the Fermi level towards the conduction band of the degenerate semiconductor and a consequent band-gap widening. A decrease in absorbance at higher doping level of Cu may be attributed to the decrease in the size of nanoparticles and increase in porosity which ultimately widens the band gap [43].

The Kubelka–Munk or remmision function is one of the better methods to determine the reflectance calculations for powder or solid samples. It is found that the absorbance coefficient ($\alpha$) is proportional to absorption and in turn absorption is proportional to reflectance, $F(R)$. Hence, $\alpha$ is replaced by $F(R)$ in the calculations. The reflectance is given by

$$F(R) = \frac{(1-R)^2}{2R}. \tag{8}$$

The band gap is calculated using the Kubelka–Munk equation [44]. In this equation $[F(R)h\nu]^2$ is plotted against $h\nu$(incident photon energy) and the extrapolated line at $[F(R)h\nu]^2 = 0$ gives the value of bandgap in electron volt (eV). The band gaps obtained are found to be 3.42, 3.50 and 3.54 eV for undoped, 1 wt% Cu doped and 3 wt% Cu doped ZnO, respectively, as shown in figure 7. Thus, the Cu doping increases the band gap of ZnO. Apparently, this change is not very large but it is significant because such small changes have also been reported for Al doping of ZnO, where drastic changes of properties have been observed [45]. The possible error range for the band gap is about $\pm 0.10\%$. The error associated with these measured gaps is extracted from the linear regression used to fit the straight lines and from the data points within the straight line region of the data [46].

The change in the optical band gap is explained in terms of Burstein–Moss (BM) band-gap widening. According to the BM effect, the donor electrons in doped semiconductors occupy states at the bottom of the conduction band. In order to conserve linear momentum, the valence electrons require additional energy to be excited to the higher energy states in the conduction band. This is as per Pauli's principle which prevents states from being doubly occupied and also because optical transitions are vertical. The band-gap shift depends on the carrier concentration in an $n$-type semiconductor [47]. Similar results have been reported for low doping indium in ZnO [48].

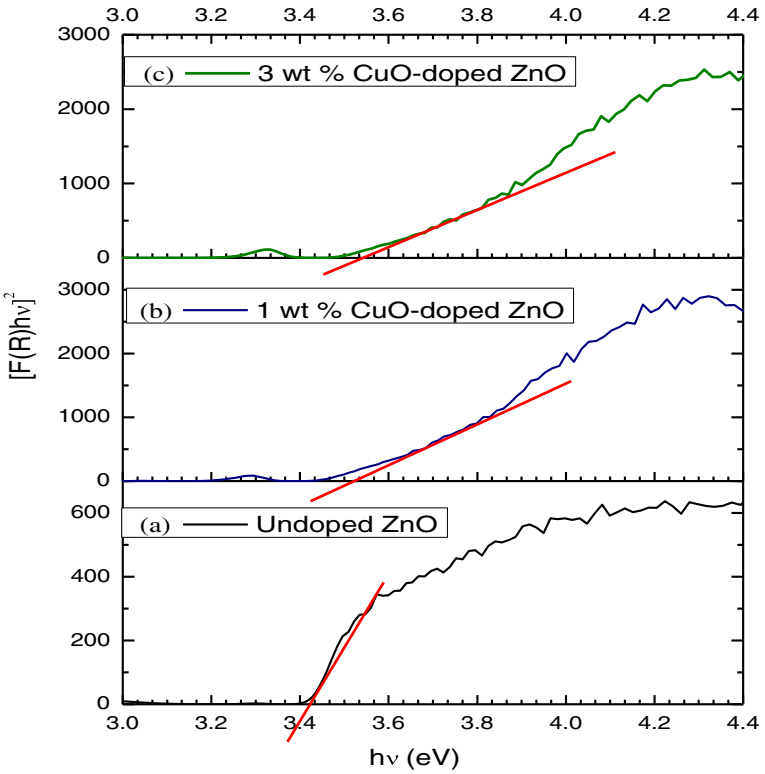


**Figure 7.** Determination of band gap for (**a**) undoped ZnO, (**b**) 1 wt% Cu-doped ZnO and (**c**) 3 wt% Cu-doped ZnO.

### 5.2 *Photoluminescence (PL) studies*

Generally, the densities of defects and oxygen vacancies significantly affect the optical properties of oxide nanostructures. The PL spectrum of undoped and Cu-doped ZnO with $\lambda_{exci} = 280$ nm is shown in figure 8. The PL spectrum of undoped ZnO exhibits strong near-band-edge emission in the region 445–475 nm. Multiple peaks are observed in the PL spectrum. The origin of these multiple peaks is attributed to carrier transitions from shallow and deep donor levels to acceptor levels of Cu ions ($Cu^{+}$ and/or $Cu^{2+}$) in ZnO. The highest intensity peak is due to excitation and the other peaks are due to the defects present in ZnO. These defects increase with Cu doping (as seen from the figure). Cu impurities provide two defect charge states, i.e., $Cu^{+}$ and $Cu^{2+}$, in the sample. The $Cu^{+}$ defects may be originated by accepting an extra electron from the nearby atom of ZnO and these defects act as shallow acceptors. At higher temperatures, $Cu^{+}$ changes to $Cu^{2+}$ or $Cu^{2+}$ thereby produces neutral copper acceptors [49]. It is also observed from the spectra that with the increase in Cu concentration, the UV emission in the Cu-doped ZnO decreases and exhibits a red-shift. As the emission at ∼458 nm is obviously lower than that of the band gap of ZnO, the visible emission cannot be ascribed to the direct recombination of a conduction electron in the Zn 3d band and a hole in the O 2p valence band [50]. The visible emission is attributed to the electron transition, mediated by defect

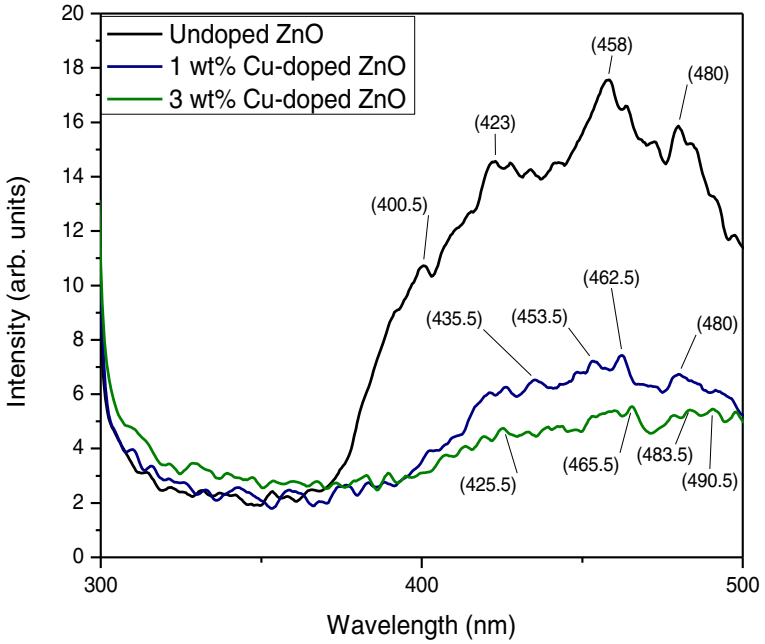


**Figure 8.** Photoluminescence spectra for undoped, 1 wt% Cu-doped and 3 wt% Cu-doped ZnO with $\lambda_{exci} = 280$ nm.

levels in the band gap. So, the intensity of the visible emission remains constant as no extra defect level is formed due to the introduction of more Cu atoms into ZnO structure.

## 6. Conclusion

The structural, electrical and optical properties of sintered ZnO and Cu-doped ZnO nanoparticles prepared by chemical method have been studied. The structural analysis confirms the formation of polycrystalline ZnO in both pure and doped samples. Change in crystallite size is observed with the increasing doping concentration of Cu. Electrical studies confirmed that the conductivity increases slightly with frequency but decreases with doping at lower concentration whereas it increases as the concentration increases. Optical studies indicate interband transitions at the fundamental edge, widening of the band gap and also red-shift with increasing Cu-dopant concentration. The results obtained in the optical studies have been analysed with the help of Kubelka–Munk equation and Burstein–Moss effect. The observations of Cu-doped ZnO reveal that this sample can be chosen as a frontier material in the study of spintronics.

## References

[1] A Dev, S Chaudhuri and B N Dev, *Bull. Mater. Sci*. **31**, 551 (2008)
[2] F A Mahmoud and G Kiriakidis, *J. Ovonic Res.* **5**, 15 (2009)

[3] N Kakati, S H Jee, S H Kim, J Y Oh and Y S Yoon, *Thin Solid Films* **519**, 494 (2010)
[4] Ch Y Wang, V Cimalla, Th Kups, C Röhlig, H Romanus, V Lebedev, J Pezoldt, Th Stauden and O Ambacher, *J. Appl. Phys.* **102**, 044310, DOI:10.1063/1.2770831 (2007)
[5] A Murali, A Barve, V J Leppert, S H Risbud, I M Kennedy and H W H Lee, *Nano Lett.* **1**, 287 (2001)
[6] G Fan, Y Wang, M Hu, Z Luo and G Li, *Meas. Sci. Technol.* **22**, 045203, DOI:10.1088/0957-0233/22/4/045203 (2011)
[7] N Van Hieu, N AnhPhucDuc, T Trung, M A Tuan and N D Chien, *Sensors and Actuators B* **144**, 450 (2010)
[8] A Azam, A S Ahmed, M S Ansari, M Shafeeq and A H Naqvi, *J. Alloys Compounds* **506**, 237 (2010)
[9] T N Soitah, Y Chunhui and S Liang, *Sci. Adv. Mater.* **2**, 534 (2010)
[10] L Sanches, J Peral and X Domenech, *Electrochima. Acta* **41**, 1981 (1996)
[11] W J Huang, G C Fang and C C Wang, *Colloids and Surfaces A: Physicochem. Eng. Aspects* **260**, 45 (2005)
[12] R Annapoorani, M R Dhanjeyan and R Renganathan, *J. Photochem. Photobiol. A: Chem.* **111**, 215 (1997)
[13] K Matsubara, P Fons, K Iwata, A Yamada, K Sakurai, H Tampo and S Niki, *Thin Solid Films* **431**, 369 (2003)
[14] Q Zhang, C Xie, S Zhang, A Wang, B Zhu, L Wang and Z Yang, *Sens. Actuators B* **110**, 370 (2005)
[15] H M Lin, S J Tzeng, P J Hsiau and W L Tsia, *Nano Struct. Mater.* **10**, 465 (1998)
[16] J Zang, W Yu and L Zang, *Phys. Lett. A* **299**, 276 (2002)
[17] S H Keshmiri and M Rezaee Rokn-Abadi, *Thin Solid Films* **382**, 230 (2001)
[18] G Singh, S B Shrivastava, D Jain, S Pandya, T Shripathi and V Ganesan, *Bull. Mater. Sci.* **33**, 581 (2010)
[19] Y Nakata, T Okada and M Maeda, *Appl. Surface Sci.* **197**, 368 (2002)
[20] Y Z Yoo, Z W Jin, T Chikyow, T Fukumura, M Kawasaki and H Koinuma, *Appl. Phys. Lett.* **81**, 3798 (2002)
[21] B J Chen, X W Sun, C X Xu and B K Tay, *Physica E* **21**, 103 (2004)
[22] Y J Li, R Duan, P B Shi and G G Qin, *J. Crystal Growth* **260**, 309 (2004)
[23] W L Dai, Y Cao, L P Ren, X L Yang, J H Xu, H X Li, H Y He and K N Fan, *J. Catalysis* **229**, 80 (2004)
[24] X S Wang, Z C Wu, J F Webb and Z G Liu, *Appl. Phys. A: Mater. Sci. Process.* **77**, 561 (2003)
[25] L M Fang, X T Zu, Z J Li, S Zhu, C M Liu, W L Zhou and L M Wang, *J. Alloys Compounds* **454**, 261 (2008)
[26] W H Zhang, W D Zhang and J F Zhou, *J. Mater. Sci.* **45**, 209 (2010)
[27] H Abdullah, M N Norazia, S Shaari, M Z Nuawi and N S Mohamed Dan, *Am. J. Eng. Appl. Sci.* **3**, 171 (2010)
[28] B D Cullity, *Elements of X-ray diffractions* (Addison-Wesley, Reading, MA, 1978)
[29] G Srinivasan, R T R Kumar and J Kumar, *J. Sol-Gel Sci. Technol.* **43**, 171 (2007)
[30] S Singhal, J Kaur, T Namgyal and R Sharma, *Physica B* **407**, 1223 (2012)
[31] I Khan, S Khan, R Nongjai, H Ahmed and W Khan, *Opt. Mater.* (2013) (in press)
[32] V Biju, S Neena, V Vrinda and S L Salini, *J. Mater. Sci.* **43**, 1172 (2008)
[33] R Ondo-Ndong, G Ferblantier, F Pascal-Delannoy, A Boyer and A Foucaran, *Microelectron. J.* **34**, 1087 (2003)
[34] D J Nagaraju and S B Krupanidhi, *Mater. Sci. Eng. B* **133**, 70 (2006)
[35] P P Sahay, S Tewari and R K Nath, *Cryst. Res. Technol.* **42**, 275 (2007)
[36] Y W Hong and J H Kim, *Ceram. Int.* **30**, 1307 (2004)
[37] M Andres-Verges and A R West, *J. Electroceram.* **1**, 125 (1997)

[38] J Jose and M A Khadar, *Nanostruct. Mater.* **11**, 1091 (1999)
[39] E J Abram, D C Sinclair and A R West, *J. Electroceram.* **10**, 165 (2003)
[40] N R Yogamalar, R Srinivasan, A Vinu, K Ariga and A Chandra Bose, *Solid State Commun*. **149**, 1919 (2009)
[41] Z Penga, X Fub, Y Zanga, Z Fua, C Wanga, L Qic and H Miao, *J. Alloys Compounds* **508**, 494 (2010)
[42] J F Wang, W B Su, H C Chen, W X Wang and G Z Zang, *J. Am. Ceram. Soc.* **88**, 331 (2005)
[43] S Tewari and A Bhattacharjee, *Pramana – J. Phys.* **76**, 153 (2011)
[44] D Bao, X Yao, N Wakiya, K Shinozaki and N Mizutani, *Appl. Phys. Lett.* **79**, 3767 (2001)
[45] P Chetri and A Choudhury, *Physica E* **47**, 257 (2013)
[46] S C Das, R J Green, J Podder, T Z Regier, G S Chang and A Moewes, *J. Phys. Chem. C* **117**, 12745 (2013)
[47] A Alaeddine, I Rachidi, F Bahsoun, Y Mohanna, O Bazzi and F El Haj Hassan, *J. Appl. Sci.* **9**, 1588 (2009)
[48] G Singh, S B Shrivastava, D Jain, Swati Pandya, T Shripathi and V Ganesan, *Bull. Mater. Sci*. **33**, 581 (2010)
[49] K Das, S Ray, S Chaudhuri and A B Maity, *Indian J. Pure Appl. Phys.* **47**, 377 (2009)
[50] E Burstein, *Phys. Rev*. **93**, 632 (1954)